Stereochemical and Angular Momentum Constraints in the Photodissociation of Ammonia

M. N. R. Ashfold, R. N. Dixon, S. J. Irving, H.-M. Koeppe, W. Meier, J. R. Nightingale, L. Schnieder and K. H. Welge

Email alerting service	Receive free email alerts when new articles cite this article - sign up in the box at the top right-hand corner of the article or click **here**

To subscribe to *Phil. Trans. R. Soc. Lond. A* go to: **http://rsta.royalsocietypublishing.org/subscriptions**

Stereochemical and angular momentum constraints in the photodissociation of ammonia

BY M. N. R. ASHFOLD[1], R. N. DIXON[1], S. J. IRVING[1], H.-M. KOEPPE[2],
W. MEIER[2], J. R. NIGHTINGALE[1], L. SCHNIEDER[2] AND K. H. WELGE[2]

[1] *School of Chemistry, University of Bristol, Bristol BS8 1TS, U.K.*
[2] *Fakultät für Physik, Universität Bielefeld, D-4800 Bielefeld 1, F.R.G.*

Time-of-flight spectra of the nascent H atoms, and laser induced fluorescence excitation spectra of the nascent NH_2 radicals, are leading to a very complete knowledge of the energy disposal following photodissociation of NH_3 through its $\tilde{A}^1A_2''$ excited state. Both the dissociation rates and the product distributions are sensitive to the values of the vibrational and rotational quantum numbers of the quasi-bound levels of the parent molecule. The most populated fragment states involve the a-axis rotational, and bending vibrational, motions of the NH_2 with modest excitation of further rotational degrees of freedom at low internal energy. For most NH_2 internal states the accompanying H atoms recoil close to the initial plane of NH_3 excitation, but for a specific subset of product states the H atoms recoil perpendicular to this plane. These measurements and their interpretation give a detailed insight into the intramolecular motion of the dissociating NH_3 molecule, which is dynamically controlled but yet involves most of the internal degrees of freedom.

1. Introduction

Photodissociation processes that are fully state resolved in both the parent molecule and the resulting products provide the most detailed insight possible into the dynamics of unimolecular reactions. Ammonia in its $\tilde{A}^1A_2''$ excited state is one model system with properties appropriate for this purpose. Earlier spectroscopic studies (Douglas 1963; Ashfold *et al.* 1986; Ziegler 1988) have characterized the energy level pattern and excited state lifetimes for this state. Recently we have presented kinetic energy distributions for the hydrogen atomic fragments resulting from photodissociation through seven different vibronic states of NH_3, and four of ND_3 (Biesner *et al.* 1988, 1989). Analysis of these kinetic energy distributions showed the accompanying NH_2 (ND_2) fragments to be formed with high levels of rotational excitation specifically concentrated about the a-inertial axis; and with increasing bending vibrational excitation for increasing excitation of the inversion vibration in the parent molecule.

Model calculations based on *ab initio* potential energy surfaces for the $\tilde{A}$ and $\tilde{X}$ states of ammonia (Rosmus *et al.* 1987; McCarthy *et al.* 1987) highlight the importance of a conical intersection of these surfaces along the $R(H_2N-H)$ dissociation coordinate in establishing the product energy distribution. The planar $\tilde{A}$ state of ammonia is quasi-bound, and dissociation from its lower vibrational levels is initiated by quantum tunnelling through a barrier, with rates that are sufficiently

[187]

slow to permit transient quantized rotation. While planarity is retained the $\tilde{A}$ state correlates smoothly with the lowest energy dissociation products $H + NH_2$ ($\tilde{X}^2B_1$), passing through the centre of the conical intersection on the way. However, for non-planar NH_3 the $\tilde{A}$ state correlates asymptotically with the excited products $H + NH_2$ ($\tilde{A}^2A_1$). This channel is energetically closed for the lower vibrational levels of $\tilde{A}$ state NH_3. The consequent 'funnelling' through the conical intersection of trajectories originating from non-planar configurations provides the strong forces which accompany non-adiabatic transfer to the $\tilde{X}$ state surface. These set up the product rotation by amplification of out-of-plane kinetic energy from the inversion motion in the inner well.

These earlier studies had insufficient resolution to prevent significant overlap in the internal energy spectra, so that the product population distributions were not revealed in full detail. There was also evidence, both experimental (Ashfold *et al.* 1985; Biesner *et al.* 1988) and theoretical (Dixon 1989), that the dissociation rate and product distribution is sensitive to the rotational state of the excited NH_3.

In this paper we present new results based on the use of improved experimental techniques, which have enabled us to characterize the product distributions in more detail than before. Stereochemical information on the dissociation process is revealed for the first time. The influence of parent rotational motion has also been investigated further.

2. Experimental

Two complementary techniques have been used in obtaining the results presented in this work. The $NH_2(\tilde{X})$ product state population distributions, and information about the angular distribution of these fragments, were measured in Bielefeld using the most recent variant of the technique of H atom photofragment translational spectroscopy. The essentials of this technique have been summarized previously (Krautwald *et al.* 1986; Schnieder *et al.* 1990), and only key features are outlined here. An internally cold sample of NH_3 was prepared using a skimmed supersonic expansion (typically 1% NH_3 in Ar, stagnation pressure not greater than 1 bar†) and photodissociated 60 mm downstream from the nozzle. The necessary photolysis wavelengths, in the range 213–217 nm, were obtained either by frequency mixing (doubled dye plus Nd–YAG fundamental) in KDP or by frequency doubling the output of the dye laser in BBO. The electric vector of this linearly polarized photolysis radiation could be set either parallel or perpendicular to the time-of-flight (TOF) axis by rotating a half wave plate. As previously (Schnieder *et al.* 1990), the nascent H atom photofragments were promoted to a high n Rydberg state using a two colour, two photon excitation via the $n = 2$ state. The Lyman α radiation necessary for the first step of this double resonance excitation scheme was obtained by frequency tripling (in krypton) the 364.6 nm output on an excimer pumped dye laser. A second pulsed dye laser, simultaneous with the first, and tuned to 364.886 nm was used to further excite these 2p H atoms to the $n = 90$ Rydberg state. The Rydberg atoms so produced 'fly' from the interaction volume to a detector (Johnston multiplier, type MM1-SG) positioned 419.8 mm away; immediately before striking this detector they are field ionised upon passing through a biased grid. A pair of suitable biased grids either side of the interaction region ensures that any ions formed by the initial laser excitations are removed at source and do not contribute to the measured TOF spectrum.

† 1 bar = 10^5 Pa.

The complementary experiments done in Bristol have used a frequency doubled Nd–YAG pumped dye laser to provide the same range of photolysis wavelengths required for exciting the 2^n ($n = 0, 1$) vibronic levels of NH_3 ($\tilde{A}$) and a second, counterpropagating dye laser to excite laser induced fluorescence (LIF) of the nascent $NH_2(\tilde{X})$ fragments. Both jet-cooled (pulsed molecular beam of neat NH_3) and bulk (low pressure static cell) samples were investigated in this way. Several types of spectra were recorded for both bulk and beam samples. LIF excitation spectra of the nascent $NH_2(\tilde{X})$ fragments were obtained by scanning the probe laser wavelength and monitoring the red-shifted $NH_2(\tilde{A} \to \tilde{X})$ fluorescence. This type of spectrum, and dispersed emission spectra obtained using a monochromator to resolve the LIF from any particular excited rovibronic state of NH_2, have provided much new spectroscopic information on the $NH_2(\tilde{A}–\tilde{X})$ system (Dixon *et al.* 1990); this data was an essential prerequisite for the present dynamical studies. Of more immediate relevance to the present work are the parent excitation spectra for forming any particular quantum state of the $NH_2(\tilde{X})$ product. These were obtained by fixing the probe laser to the (known) $NH_2(\tilde{A}–\tilde{X})$ rovibronic transition of interest and monitoring the resulting LIF intensity whilst tuning the wavelength of the linearly polarized photolysis laser (with ϵ_{phot} arranged either parallel or perpendicular to ϵ_{probe}).

3. Assignment of the H-atom time of flight spectra

The higher resolution afforded by the Rydberg atom excitation technique compared with the earlier prompt ionization technique has resulted in time of flight spectra that show considerably more detail than before (Biesner *et al.* 1988, 1989). In particular, it is now evident that the peaks cannot solely be assigned to fragmentation to NH_2 levels with $N = K_a$. Furthermore, the relative intensities of the various peaks in these spectra have been found to vary with the geometry of detection of the H atoms relative to the polarization of the photolysis radiation, as well as with the quantum state of NH_3 through which dissociation is initiated. Figure 1 *a–d* presents such spectra (transformed to the scale of NH_2 internal energy) for dissociation within the NH_3 $\tilde{A}–\tilde{X}$ 0_0^0 and 2_0^1 bands.

The peaks in these spectra were assigned using a combination of experimental and theoretical information. With knowledge from our earlier work of the type of levels populated in the fragment NH_2 we have been able to assign much of the visible LIF spectrum of the nascent NH_2. This in turn, together with other spectroscopic data (M. Vervloet, personal communication), has enabled us to refine the model for calculation of high K_a states. Figure 2 gives detailed assignments for the NH_2 internal energy spectrum recorded following photolysis through the 2_0^1 band with detection of H atoms perpendicular to the electric vector. This is one of the more richly structured spectra. The strongest peaks are indeed those with $v_2 = 0$ and $N = K_a$ for the nascent NH_2 as deduced previously. However, at low fragment internal energy the $N = K_a + 1$ levels have almost equal population to those with $N = K_a$. Furthermore, many levels are observed with $v_2 = 1$ or 2.

(a) *Stereochemical aspects of dissociation through the 0_0^0 band*

Time-of-flight spectra have been recorded through photolysis of a cold (*ca.* 20 K) beam of NH_3 at 46 148 cm^{-1} and at 46 197 cm^{-1} within the 0_0^0 band, and in both polarizations. Figure 1 *a, b* shows two of the corresponding NH_2 internal energy spectra. All of these spectra are dominated by peaks associated with the $N = K_a$,
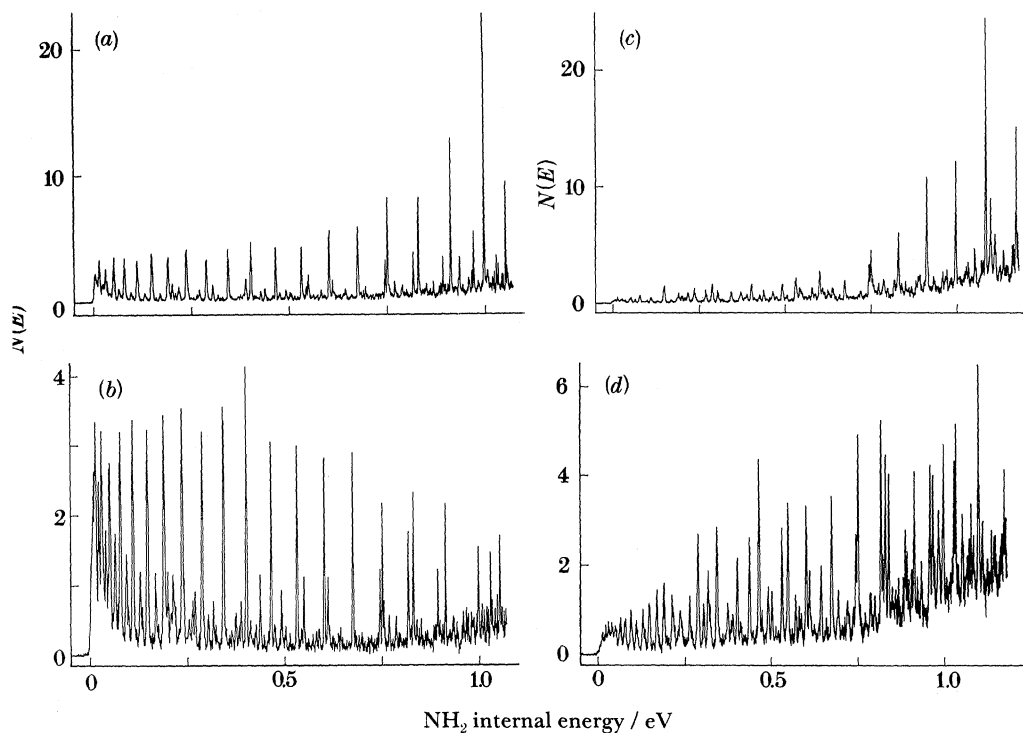
378 *M. N. R. Ashfold and others*

Figure 1. NH_2 internal energy spectra from photolysis of NH_3 in the $\tilde{A}$–$\tilde{X}$ bands at; (a) 46 197 cm^{-1} (0_0^0 band) with detection of the H atoms parallel e_{phot}; (b) 46 197 cm^{-1} in perpendicular polarization; (c) 47 110 cm^{-1} (2_0^1 band) in parallel polarization; (d) 47 110 cm^{-1} in perpendicular polarization.
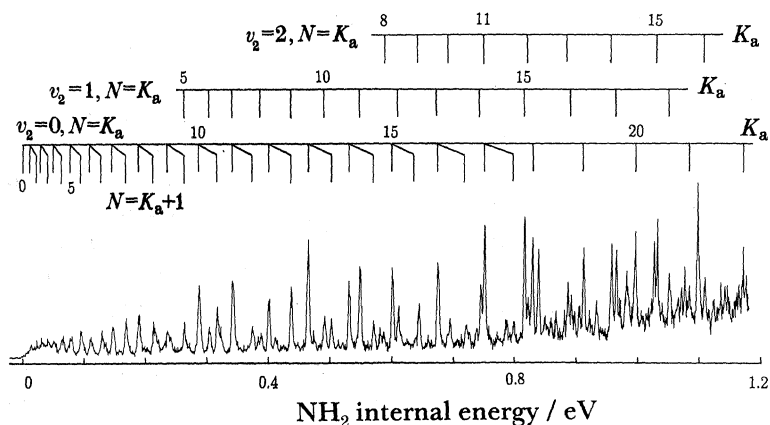

Figure 2. Assignments of the structure in the spectrum of figure 1d.

$v_2 = 0$ levels of the NH_2 fragment, with N ranging from 0 to 20; with weaker series for $N = K_a$, $v_2 = 1$ from $N = 0$ to 18, a few high $N = K_a$ levels with $v_2 = 2$, and a series of peaks for $N = K_a + 1$, $v_2 = 0$ levels with N up to about 10. The significant variations in relative intensity with both excitation frequency and polarization can be summarized as follows.

[190]

1. In perpendicular polarization there is a general fall in intensity with increasing N, but a rise with N in parallel polarization. These trends are much more pronounced at $46\,197$ cm^{-1} than at $46\,149$ cm^{-1}.

2. The intensities of the $N = K_a + 1$, $v_2 = 0$ peaks relative to those with $N = K_a$ increase by a factor of about two when the excitation wavenumber is increased from $46\,148$ to $46\,197$ cm^{-1}.

Trend 1 indicates that the recoil anisotropy parameter β becomes more positive as N increases. To place this variation on an absolute basis we have endeavoured to establish the relative sensitivities of detection in the two polarizations. Figure $3\,a$, b gives the best estimates of the absolute ratio $I_{\parallel}/I_{\perp}$ for the $N = K_a$, $v_2 = 0$ levels at the two excitation frequencies. In both cases this ratio is less than 1 at low N but is greater than 1 at high N. As

$$\beta = 2(I_{\parallel} - I_{\perp})/(I_{\parallel} + 2I_{\perp}), \tag{3.1}$$

this implies that β is negative at low N and positive at high N, with limiting values at $46\,197$ cm^{-1} of $\beta \approx -0.4 \pm 0.2$ and $\beta \approx +0.8 \pm 0.4$ respectively. β is much closer to zero at $46\,148$ cm^{-1}.

Linearly polarized light produces an aligned sample of excited state molecules, and for very short excited state lifetimes the alignment parameter $\mathscr{A}_0$ for the transition dipole has the limiting value of $+2$, corresponding to a pure $\cos^2 \theta$ distribution in space. For the present case, where the NH_3 $\tilde{A}$–$\tilde{X}$ bands have a parallel transition moment, $\mathscr{A}_0$ relates to the alignment of the top axis. β is related to $\mathscr{A}_0$ through the molecular frame distribution of final recoil,

$$\beta = \mathscr{A}_0 \langle P_2(\cos \theta_m) \rangle, \tag{3.2}$$

where θ_m is the polar angle in the molecular frame. Thus to assess the dynamical significance of the measured values of β we must know $\mathscr{A}_0$ as a function of excitation frequency, and since the $\tilde{A}$ state of NH_3 has some semblance of rotational structure this is not necessarily the limiting value of $+2$. For resolved rotational levels $\mathscr{A}_0$ can be calculated from the rotational wavefunctions and the Hönl–London factors.

Two broadened rotational transitions (FWHM ≈ 38 cm^{-1}) lie close to $46\,197$ cm^{-1}; $R_0(1)$ with $\mathscr{A}_0 = +1.0$, and $R_1(1)$ with $\mathscr{A}_0 = +0.5$, with intensities in the ratio of about $2:1$ at 20 K. The mean excitation therefore yields $\mathscr{A}_0 \sim +0.83$. Combining this value of $\mathscr{A}_0$ with the experimental values of β given above, we deduce that the alignment in the molecular frame, $\langle P_2(\cos \theta_m) \rangle$, is close to the negative limit of -0.5 at low N, and the positive limit of $+1.0$ at high N.

$46\,148$ cm^{-1} lies closest to $P_0(1)$ at $46\,143$ cm^{-1}, with $\mathscr{A}_0 = 0$; but there will also be some excitation through overlap from $Q_1(1)$ at $46\,161$ cm^{-1}, which is almost as strong at 20 K, with $\mathscr{A}_0 = +0.5$. Thus the mean alignment will be positive but small. The much lower variation of $I_{\parallel}/I_{\perp}$ at this frequency is thus seen to be a consequence of the mode of excitation, rather than a change in dissociation dynamics with excitation frequency.

Thus we conclude that at low N the H-atom is ejected at right angles to the C_3 top axis of NH_3, but parallel to this axis at the highest N that is energetically accessible. The low N behaviour is as expected. The molecule is planar in the excited state: dissociation proceeds first by quantum tunnelling and then by passage through a conical intersection of the $\tilde{A}$ and $\tilde{X}$ surfaces in an H_2N–H exit channel, for which the molecule is also planar. In contrast, the high N behaviour can be interpreted as a consequence of angular momentum conservation. We have previously concluded
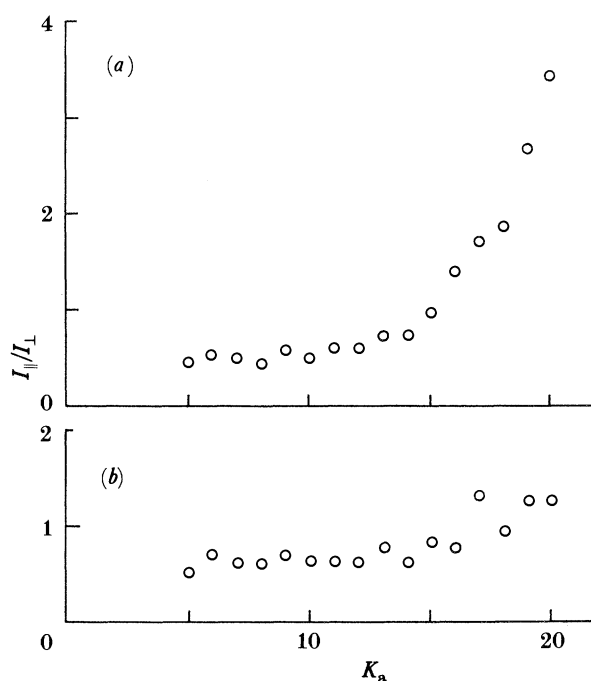
Figure 3. Best estimates of the ratios $I_\parallel/I_\perp$ of H atoms detected parallel and perpendicular to ϵ_{phot} at (a) $46\,197$ cm^{-1}, and (b) $46\,148$ cm^{-1}. (Note that some arbitrariness attaches to these ratios since the original spectra were not recorded under conditions of strictly equivalent laser intensity.)

(Biesner *et al.* 1988) that in dissociation from the origin level of the $\tilde{A}$ state most trajectories cross directly from the $\tilde{A}$ to the $\tilde{X}$ surface close to the planar conical intersection where R(H$_2$N–H) is only about 2 Å†. To generate an NH$_2$ fragment with high rotation about its *a*-axis it is necessary that the H-atom partner develop a high orbital angular momentum about an axis perpendicular to the NH$_3$ top axis. Given that R is small, this is most probably achieved by motion parallel to the top axis.

It should be stressed that the values of $\mathscr{A}_0$ calculated above ignore any contributions from the coherent excitation of P, Q and R transitions from any given level, which may be possible given their widths. This neglect may have a quantitative significance, but should not alter the qualitative conclusions.

Trend 2 may arise from a separate consequence of angular momentum conservation. In a non-rotating parent molecule the angular momentum of an NH$_2$ fragment will be entirely generated by potential forces, the symmetry of which will favour $N = K_a$ fragment states. However, neither excitation frequency generates $J' = 0$ exclusively. At $46\,197$ cm^{-1} both excited states have $J' = 2$, with some angular momentum about each of the three top axes. Thus whichever NH bond breaks, there will be some distribution of initial angular momentum perpendicular to the *a*-axis of the resultant NH$_2$ fragments, which would favour $N > K_a$. But the rotational energy associated with the perpendicular component of rotation for the NH$_2$ levels is $\bar{B}K_a$ for $N = K_a$, $\bar{B}(3K_a+2)$ for $N = K_a+1$, and $\bar{B}(5K_a+6)$ for $N = K_a+2$. Thus on energetic grounds the population of $N > K_a$ levels should fall with increasing K_a, as observed. At $46\,148$ cm^{-1} the principal excitation is to $J' = 0$, with weaker excitation

† 1 Å $= 10^{-10}$ m $= 10^{-1}$ nm.

[192]

to $J' = 1$, thus explaining the weaker excitation of NH_2 levels with $N > K_a$ at this frequency.

We will return to the topic of angular momentum conservation in a later section.

(b) *Dissociation through the 2_0^1 band*

At 20 K the $R_0(0)$ transition of 2_0^1 centred around 47069 cm^{-1} is by far the strongest feature, so that the band shows a single peak (this transition is absent from the 0_0^0 band because of nuclear statistics). This transition is the only one for which $\mathscr{A}_0$ has the limiting value of $+2$ for a symmetric top irrespective of excited state lifetime. Experimentally we have found little variation in the time-of-flight spectra recorded on the maximum, or in either wing, of this peak. Figure 1*c*, *d* shows that the high $N = K_a$, $v_2 = 0$ peaks show the same relative increase in parallel polarization as in the spectra recorded via the 0_0^0 band, which we may again attribute to angular momentum conservation at the crossing of the conical intersection of the $\tilde{A}$ and $\tilde{X}$ potentials. As noted earlier (Biesner *et al.* 1988, 1989), these high $N = K_a$, $v_2 = 0$ states indicate a strong population inversion, which has been shown to arise from amplification at the conical intersection of the momentum initially present in the quantum of inversion vibration.

However, the most striking observation is that the spectrum is parallel polarization consists almost entirely of this series of $v_2 = 0$ peaks at high internal energy, whereas the perpendicular spectrum has a much richer structure, which spans a much wider energy range. Thus for the majority of the fragment levels the H atom departs perpendicular to the top axis, that is in the NH_3 plane. At this angle there is almost equal population of equivalent N levels for $v_2 = 0$ and 1, and a significant population in $v_2 = 2$ (see figure 2). Furthermore, at low K_a there is equal population of the $N = K_a$ and $N = K_a + 1$ levels, but only for $v_2 = 0$.

Our interpretation of these latter observations is necessarily somewhat speculative in the absence of a detailed knowledge of the variation of the potential energy surfaces with all the internal coordinates. We start by noting that the 2^1 level possesses a vibrational energy of *ca.* 900 cm^{-1}, and in comparison with the zero-point level has opposite symmetry to inversion in the molecular plane. Thus in the non-rotating parent molecule this quantum only becomes available to the products in the exit channel, where the potential hindering inversion motion disappears. The symmetry is lowered in a rotating frame, but it is not immediately obvious that excitation to $J' = 1$ should cause any significant change.

But we have not yet considered the total set of degrees of freedom of the dissociating molecule. In particular, we do not know the frequency of the in-plane e' bending vibration ν_4': in the $\tilde{X}$ state of ammonia $\nu_4'' = 1627$ cm^{-1}. On dissociation, one component of ν_4' will be asymptotic to the bending frequency $\nu_2 = 1497$ cm^{-1} of NH_2, while the other component is a disappearing mode which correlates with *c*-axis rotation of the NH_2. The first of these components has a_1 symmetry in the C_{2v} point group of planar H_2N–H as reference, and will have the same a' symmetry as ν_2' upon further distortion to a non-planar C_s point group. Rosmus *et al.* (1987) have already noted that the H_2N–H internuclear distance at the $\tilde{A}$–$\tilde{X}$ conical intersection is a strongly varying function of the NH_2 angle. Thus in the vicinity of this intersection there are strong forces which couple the radial coordinate, the inversion motion, and NH_2 bending, thus providing a mechanism for interchange of energy between the initially excited inversion quantum and NH_2 bending.

Since the HNH angle in planar NH_3 is $120°$, but is $104°$ and $144°$ respectively in

the $\tilde{X}$ and $\tilde{A}$ states of NH_2, we may ask why this energy transfer should be important for excitation in the 2_0^1 band of ammonia, but not in the 0_0^0 band. As noted above, our earlier classical trajectory calculations on the Rosmus surface showed that for the zero-point level most trajectories lead to dissociation on the first approach to the conical intersection; but for the 2^1 level there was an increasing proportion of indirect trajectories which sample a wider range of the potential energy surfaces (Biesner *et al.* 1988). Promotion of the ν_2'/ν_4' energy transfer will be enhanced by increasing v_2', and thus the proportion of indirect trajectories. On this basis we would expect that the excitation of ν_2 in NH_2 would increase with increase in v_2' of NH_3, in accordance with observation (Biesner *et al.* 1989).

These considerations also lead to an understanding of the polarization behaviour. Direct dissociation at the first crossing of the conical intersection results in the final product motion being established near $R(H_2N-H) = 2$ Å. For high $N = K_a$ states inertial constraints and angular momentum conservation will then be best satisfied if the H atom velocity vector lies close to the initial top axis, leading to preferential detection in parallel polarization, as argued above. However, this could be the exception rather than the rule, and may only be of importance for trajectories that lead to $v_2(NH_2) = 0$. In all other cases the final product motion may not be established until a much larger value of R. Inertial constraints will then bias the H atom motion to being much closer to perpendicular to the top axis, giving preferential detection in perpendicular polarization.

Finally, we come to the increased ratio of $N = K_a + 1$ to $N = K_a$ states upon photolysis via 2_0^1. From the above remarks it will be noted that $\nu_4'(e', b_2$ in $C_{2v})$ is probably greater than ν_2' at short R, but falls to zero at large R. Thus these modes will come into resonance at some intermediate value of R. Coriolis forces about an axis perpendicular to the top axis have the correct symmetry to couple these modes, thereby promoting transfer of the $v_2' = 1$ quantum into $v_4' = 1$ and thus to rotation of the NH_2 about an axis perpendicular to its a-axis. This in turn will populate $N > K_a$ states, but only for $v_2(NH_2) = 0$ as observed. This mechanism necessarily requires NH_3 rotation ($J' = 1$ in the present case), and would increase in importance as J increases with $J \gg K$. Unfortunately, there is no $J = 0$ state for the 2^1 vibronic level because of nuclear statistics, so that it is impossible to test this hypothesis by exciting a non-rotating ammonia molecule.

4. The influence of NH_3 angular momentum and rotational energy

The intensity distribution in the action spectrum for producing a given internal energy state of a photofragment is a product of the parent absorption spectrum and the excited state branching ratio to that state. Such action spectra have been recorded over the 0_0^0 band using a room temperature sample of NH_3 for many different NH_2 states; and over both the 0_0^0 and 2_0^1 bands using a jet-cooled sample and a few NH_2 states. Each of these spectra was power normalized. Examples are given in figure 4*a, c, d*. Most of the room temperature 0_0^0 spectra are fairly similar to figure 4*a*. However, there are some significant variations from one fragment state to another under equivalent experimental conditions, indicating variable branching ratios. To aid interpretation of these effects, comparisons have been made with simulations of the NH_3 absorption bands for various assumed temperatures.

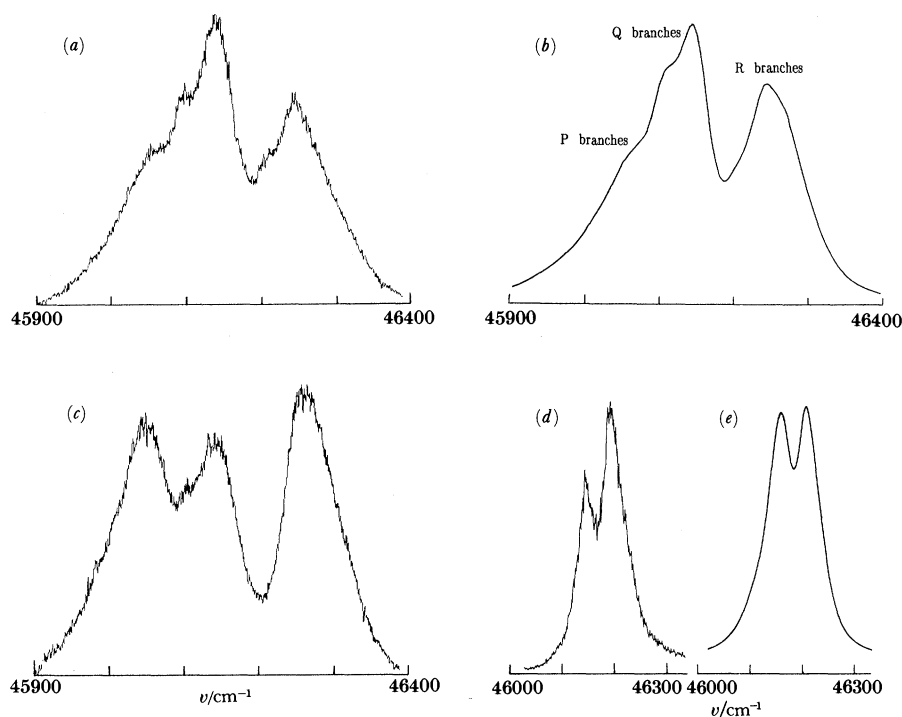Variable branching ratios can arise from two causes. As the laser is tuned across

Figure 4. Action spectra of NH_3 for producing a specific internal energy state of NH_2, detected through LIF excitation of the NH_2 product. (a) Photolysis of room temperature NH_3, with detection via the $^PP_{15}(15)$ 2_0^1 transition at $17\,777$ cm^{-1}; (b) the calculated NH_3 ($\tilde{A}$–$\tilde{X}$) 0_0^0 absorption band at 290 K in simulation of (a); (c) photolysis of room temperature NH_3, with detection via $^PP_{21}(21)$ 0_0^0 at $17\,741$ cm^{-1}; (d) photolysis of a jet cooled sample of NH_3, with detection via $^RR_{20}(20)$ 0_0^0 at $19\,490$ cm^{-1}; (e) the calculated NH_3 ($\tilde{A}$–$\tilde{X}$) 0_0^0 absorption band at 50 K in simulation of (d).

the parent absorption spectrum different rotational branches are accessed, so that the total energy in the parent molecule may vary by far more than the change in laser frequency. The resultant change in available energy may open new fragment states that are close to threshold for the non-rotating parent molecule. Secondly, the angular momentum of the parent molecule may influence the dissociation dynamics through the effects of centrifugal or Coriolis forces. Clearly both these mechanisms will be more developed in room temperature spectra than in a beam because of the wider range of rotational state population. However, the predissociation width of 30–40 cm^{-1} make it impossible to excite a single quantum state under almost all circumstances.

We first discuss action spectra of the 0_0^0 band. Room temperature spectra recorded using visible transitions of NH_2 originating in levels with $N = K_a$, $v_2 = 0$ and $N = 9$, 10, 11, 15, 16 or even 20 are all very similar, and closely resemble the simulated absorption band (see figure 4a, b). Thus in these cases there is no apparent variation of the branching ratio with the rotational state of NH_3. The NH_2 fragment states probed in these cases are all removed from the limit of the available energy. In contrast, the action spectrum recorded when probing the $^PP_{21}(21)$ 0_0^0 transition of NH_2 at $17\,741$ cm^{-1} has a very different profile (figure 4c). Whereas the P and Q branches of the NH_3 band usually overlap to the extent that each $\tilde{A}$–$\tilde{X}$ absorption band shows just two peaks in the regions of the Q and R branches, in this case there

Phil. Trans. R. Soc. Lond. A (1990)

are three separate peaks with the Q peak slightly weaker than the other two. Thus Q branch transitions lead to a lower branching ratio for the $N = K = 21$ state of NH_2 than do the P and R branch transitions. This effect was observed to be independent of laser polarizations. We note at this point that this NH_2 transition is hardly visible in an NH_2 LIF spectrum recorded from dissociation in a cooled beam, but is quite strong at room temperature.

A similar weakening of the Q branch is apparent in the action spectrum of the 0_0^0 NH_3 band recorded in a cooled beam when probing the $^RR_{20}(20)$ 0_0^0 NH_2 line at 19490 cm^{-1}, (figure $4d$) when comparison is made with simulations. From many experiments using expanding beams of neat NH_3 and fully resolvable spectra we have observed rotational equilibrium in the ground state at 45–50 K (which is close to the thermodynamic limit). At this temperature the simulated band has two peaks of closely similar intensity (figure $4e$); the first at *ca.* 46155 cm^{-1} principally made up of one P transition and three Q transitions, and the second at *ca.* 46205 cm^{-1} consisting only of R transitions, (higher J P-branch transitions are very weak at this temperature). Any increase in temperature strengthens the Q peak relative to the R peak. But experimentally the Q peak is considerably weaker than the R peak.

We seek an understanding of the energetic and angular momentum effects on the branching ratios to these fragment states. The total energy available to the fragments from a given rotational state of NH_3 is:

$$E_{av}(J'K') = T_{00} + B'J'(J'+1) - (B'-C')K'^2 - D_0^0. \qquad (4.1)$$

In principle a fragment channel is open if $E_{av}(J'K')$ exceeds $E_{int}(NH_2)$. However, angular momentum conservation has the consequence that there is a centrifugal barrier in dissociation to NH_2 states of high N. This is best explored through the rotational terms in the potential for H interacting with NH_2.

Let R be the reaction coordinate, I_a, I_b and I_c the instantaneous moments of inertia for NH_2, l the orbital angular momentum and J the total angular momentum. The rotational terms are then

$$H_{rot} = \frac{\hbar^2}{2} \left[\frac{l^2}{\mu R^2} + \frac{(J_x - l_x)^2}{I_a} + \frac{(J_y - l_y)^2}{I_b} + \frac{(J_z - l_z)^2}{I_c} \right]. \qquad (4.2)$$

The angular momentum N for the NH_2 fragment neglecting spin is given by

$$N = J - l. \qquad (4.3)$$

Thus for a given J of NH_3, and N for NH_2, l can range from $|(J-N)|$ to $(J+N)$, the minimum centrifugal barrier being for $l = |(J-N)|$. We also note that the NH_2 fragments have $N = K_a$ or $N = K_a + 1$, so that this minimum value of l requires that J be concentrated around the x axis of NH_3. This is the case for NH_3 levels with $J \gg K$. In contrast, levels with $J \approx K$ have J concentrated around the z axis which will lead via the dominant coupling to $l = N$ for $N \gg J$ (N perpendicular to J).

The $N = K = 21$ channel of NH_2 is just closed at the origin of the 0_0^0 band ($\Delta E_{av}(0,0) = -50 \pm 85$ cm^{-1}); that for $N = K = 20$ is open by 660 ± 85 cm^{-1}. Table 1 lists values of the impact parameter b $= R_{min}$ calculated by equating $\Delta E_{av}(J,K) - E_{int}(NH_2)$ to the centrifugal energy, using $l = (N-J)$ for levels with $K = 0$ and $l = N$ for $J = K$.

High angular momentum states of NH_2 in $v_2 = 0$ become populated during the dissociation as the evolving wavefunction passes the conical intersection between the $\tilde{A}$ and $\tilde{X}$ surfaces of ammonia near $R \approx 2$ Å, reaching their asymptotic probabilities

Table 1. *Impact parameters for photofragmentation of the* $\tilde{A}(v = 0)$ *state of* NH_3 *to* $H + NH_2$

	NH₂ level			
	$N = K_a = 20$		$N = K_a = 21$	
NH₃ level	$\Delta E_{av}/cm^{-1}$	$b/\text{Å}$	$\Delta E_{av}/cm^{-1}$	$b/\text{Å}$
$J, K = 0, 0$	657	3.37	-50	—
1, 0	676	3.16	-30	—
2, 0	716	2.91	8	29
3, 0	774	2.65	67	9.5
4, 0	852	2.38	144	6.14
5, 0	949	2.12	242	4.47
6, 0	1066	1.87	358	3.45
7, 0	1202	1.64	494	2.75
8, 0	1357	1.43	650	2.23
$J, K = 1, 0$	672	3.33	-35	—
2, 2	696	3.28	-11	—
3, 3	749	3.20	22	19
4, 4	773	3.11	66	11
5, 5	825	3.01	118	8.3
6, 6	888	2.90	181	6.74
7, 7	960	2.79	253	5.70
8, 8	1041	2.68	334	4.96
9, 9	1132	2.57	425	4.40

by about $R \approx 3$ Å. Table 1 shows that for formation of the $N = K_a = 20$ levels of NH_2 b comes inside this range for $J > 1$ with $J = K$, or $J > 5$ if $K = 0$, and this channel is then classically open. There are regions of weak attractive potential at large R on the $\tilde{X}$ state surface, but these are not sufficient to lower the effective barrier substantially if $b > 3$ Å. The assumption that l cannot fall below N for dissociation from $J = K$ states is extreme. Nevertheless, it is clear that for a given value of J rotation about a perpendicular axis $(J \gg K)$ will be more effective in promoting dissociation to this high N fragment state than rotation about the NH_3 top axis $(J = K)$ on both energetic and angular momentum grounds. Excitation through the P or R branches favours levels with $J \gg K$ in this parallel band, whereas Q branches favour levels with $J \approx K$. This will enhance the branching ratio for P or R transitions relative to Q transitions, as is observed in the low temperature spectrum of figure 4*c*.

For $N = K_a = 21$ b never falls below 3 Å for $J < 7$, thus explaining the absence of this fragment state for dissociation in a cooled beam. At higher temperatures the channel becomes open, but we again expect preferential branching to this state via P and R transitions as observed. Conversely for $N = K_a = 19$ $b = 2.24$ Å for $J = K = 0$, so that parent rotation should have little influence on the branching ratio, which is again in agreement with experiment for this and for lower values of N.

Some action spectra of the 2_0^1 band recorded using a cooled beam show a similar enhancement of the R branch to that described above but at least one shows a dominant Q branch. However, further work is needed on the assignment of the NH_2 LIF spectrum before these can be interpreted with any confidence.

5. Conclusions

The results described in this paper reinforce and extend our earlier general conclusions concerning the dissociation mechanism of $\tilde{A}$ state NH_3 (Biesner *et al.* 1988, 1989), by providing better selectivity in the methods of detection.

Phil. Trans. R. Soc. Lond. A (1990)

The introduction of the Rydberg atom excitation method into the technique of H atom photofragment translation spectroscopy has circumvented the effects of space charge in the source region which accompany direct ionization. Not only has this led to a substantial improvement in the energy resolution of the technique, but it has also revealed polarization phenomena which were not apparent in the earlier work. LIF detection of the nascent NH_2 radicals provides further complementary information.

Dissociation from the zero point level of the $\tilde{A}$ state of NH_3 yields ground state NH_2 fragments, primarily in their zero-point level. The rotational excitation of these fragments is mainly distributed into the $N = K_a$ states, in which the NH_2 rotation is confined to motion about the a-inertial axis. At the highest values of K_a which are energetically accessible the accompanying H atom is ejected parallel to the initial C_3 top axis. However, this stereochemical behaviour appears to be limited to atoms which partner dissociation to high K_a states with $v_2(NH_2) = 0$. This we associate with direct dissociation at the first approach to the conical intersection of the $\tilde{A}$ and $\tilde{X}$ potential surfaces of ammonia. In contrast, in the norm the H atoms are ejected close to the initial plane of the NH_3 molecule, which provides evidence that forces act in the exit channel out to large values of $R(H_2N-H)$. It is also now apparent that there is some population of NH_2 states with $N > K_a$, and that this is greater for photolysis of NH_3 via the 2_0^1 band than via the 0_0^0 band.

In interpreting these observations we conclude that the important motion during the dissociation is not restricted to inversion and bond stretching, even though dissociation is initiated through excitation only of ν_2'. In-plane bending and parent rotation have both been invoked in promoting dissociation to certain of the observed product states. Thus an accurate theoretical description of the complete dissociation mechanism would necessarily have to consider all the available degrees of freedom.

References

Ashfold, M. N. R., Bennett, C. L. & Dixon, R. N. 1985 *Chem. Phys.* **93**, 293–306.

Ashfold, M. N. R., Bennett, C. L. & Dixon, R. N. 1986 *Faraday Discuss. chem. Soc.* **82**, 163–175.

Biesner, J., Schnieder, L., Schmeer, J., Ahlers, G., Xie, X., Welge, K. H., Ashofold, M. N. R. & Dixon, R. N. 1988 *J. chem. Phys.* **88**, 3607–3616.

Biesner, J., Schnieder, L., Ahlers, G., Xie, X., Welge, K. H., Ashfold, M. N. R. & Dixon, R. N. 1989 *J. chem. Phys.* **91**, 2901–2911.

Dixon, R. N. 1989 *Molec. Phys.* **68**, 263–278.

Dixon, R. N., Irving, S. J. & Nightingale, J. R. 1990 *Molec. Phys.* (Submitted.)

Douglas, A. E. 1963 *Discuss. Faraday Soc.* **35**, 158–174.

Krautwald, H. J., Schnieder, L., Welge, K. H. & Ashfold, M. N. R. 1986 *Faraday Discuss. chem. Soc.* **82**, 99–110.

McCarthy, M. I., Rosmus, P., Werner, H. J., Botschwina, P. & Vaida, V. 1987 *J. chem. Phys.* **86**, 6693–6700.

Rosmus, P., Botschwina, P., Werner, H. J., Vaida, V., Engelking, P. C. & McCarthy, M. I. 1987 *J. chem. Phys.* **86**, 6677–6692.

Schnieder, L., Meier, W., Welge, K. H., Ashfold, M. N. R. & Western, C. M. 1990 *J. chem. Phys.* (Submitted.)

Ziegler, L. D. 1988 *J. chem. Phys.* **86**, 1703–1714.